Membrane Technology
ISSN (online): 1873-4049

Hydrothermal Synthesis and Characterization of C@$ZrSiO_4$ Black Pigment Based on Mesoporous Structure Collapse of Zirconium Silicate

Junxiong Zhang[1], Wen Li[1], Junling Yu[1], Tao Wang[1], Guirong Xu[2], Feng Jiang[1,*]

[1]*Department of Material Science and Engineering, Jingdezhen Ceramic University, Jingdezhen 333000, China*

[2] *National Engineering Research Center for Domestic & Building Ceramics, Jingdezhen Ceramic University, Jingdezhen 333000, China*

**Corresponding Author.*

Abstract:

In this paper, Zirconium silicate inclusion carbon black (C@$ZrSiO_4$) pigment was prepared by mesoporous structure collapse of $ZrSiO_4$. The optimal synthesis process of C@$ZrSiO_4$ pigment was studied. The results show that mesoporous $ZrSiO_4$ with specific surface area of 322.4805 m^2/g can be obtained at 180 ℃ hydrothermal temperature. APTES can facilitate the combination of carbon black (CB) and $ZrSiO_4$, and the optimal molar ratio of APTES/Zr is 0.5364. By utilizing the special structure of layered mesopores $ZrSiO_4$, we have successfully synthetized highly chromogenic C@$ZrSiO_4$ pigment with L^* value of 27.65.

Keywords: pigments, Zirconium silicate, inclusion, carbon black, triethoxy-3-aminopropylsilane.

INTRODUCTION

With the promotion and popularity of pigments, black pigments are favored for their stable and dignified color, which are one of the most common ceramic decorations[1]. Commercial black pigments mainly consist of spinel oxide such as Co-Cr-Fe-Mn. Due to the high price of cobalt resources and the dissolution of toxic heavy metals in daily use, it is urgent to develop the low-cost and non-toxic black ceramic pigment to substitute for spinel structure based black pigments[2]. Many Studies have shown that Carbon black (CB) is the most common colorant in black pigments, which can play an important role in solving economic and environmental problems caused by tradition spinel pigment. However, CB is too easy oxidized in a high-temperature environment to be applied to ceramic decorative decoration. Therefore, encapsulated carbon black material has become the development direction of non-toxic ceramic pigment. Compared with CB, $ZrSiO_4$ has higher temperature stability and chemical stability, and it also has high refractive index. By covering the surface of CB with $ZrSiO_4$, CB can have better thermal stability and chemical stability without affecting the good tinting performance.

In the study of C@$ZrSiO_4$ black pigments, much work focused on the surface modification of the CB and the type of carbon source. In the cause of the problem of the low content of organic functional groups in conventional CB particles, it is not easy to combine with $ZrSiO_4$. Peng et al. carried out surface functional group oxidation and surface modification of CB, which improved the properties of the pigment (L^*=36.25)[3]. Furthermore, Chen et al. used sisal as a new carbon source to greatly improve its encapsulation rate, and the chroma value was reduced to 34.93[4]. Although the above two approaches can improve the performance of pigments. However, few people has noticed to the use of mesoporous $ZrSiO_4$ of hydrothermal synthesis structure collapse to enhance the properties of C@$ZrSiO_4$ black pigment.

In this work, mesoporous $ZrSiO_4$ with layered porous structure was synthetized by a hydrothermal method, which provide a good prerequisite for CB inclusion. The synthesis mechanism of C@$ZrSiO_4$ black pigment was investigated by X-ray photoelectron spectroscopy (XPS), transmission electron microscope (TEM), scanning electron microscope (SEM) and other testing analysis. Meanwhile, the prepared pigment also has a good color rendering performance in the glaze.

EXPERIMENTAL

Preparation of Mesoporous $ZrSiO_4$

Mesoporous $ZrSiO_4$ was prepared by hydrothermal method that Zirconium oxychloride octahydrate ($ZrOCl_2 \cdot 8H_2O$, AR, Aladdin), tetraethoxysilane (TEOS, AR, Aladdin) as zirconium source and silicon source, LiF as mineralizer, and deionized (DI) water as solvent. Above all, 0.3 mol/L $ZrOCl_2 \cdot 8H_2O$ was entered into DI water and stirred to dissolve Zr source. LiF was added to solution which was stirred until sol was formed. Further, 0.36 mol/L TEOS was dropped into the sol. Then add ammonia water to make the sol pH 9 to obtain the $ZrSiO_4$ precursor. Whereupon, the precursor was dumped into a high-pressure autoclave at 180 ℃ for 24 h for complete reaction. After the reaction, the samples was dried at 60 ℃ for 12 h to gain mesoporous $ZrSiO_4$.

Preparation of C@$ZrSiO_4$ Pigment

Figure 1 show a sketch of fabrication approach to C@$ZrSiO_4$ black pigment. First, prepare solution according to the above method. Meantime, vary triethoxy-3-aminopropylsilane (APTES) contents were determined in molar ratio of APTES/Zr=0, 0.1788, 0.3576, 0.5364, 0.7152 and then was added into 8 mL Carbon ink under the action of magnetic mixer to obtain mixed liquid. Subsequently, add all mixed liquid to Zr precursor solution to obtain sol. And further 0.9 mol/L LiF and 0.36 mol/L TEOS dissolve in sol. The sol was adjusted pH to 9 by dropping ammonia water to derive precursor solution. After that, the precursor solution was transferred to high-pressure autoclave of 100 mL capacity to obtain C/$ZrSiO_4$ at 180 ℃ for 24 h. Subsequently, the obtain C/$ZrSiO_4$ was dried at 60 ℃ for 24 h. Finally, the as-prepared C/$ZrSiO_4$ samples by specially treated were calcined at 900 ℃ for 2 hours. Mix the obtained pigment mixture with molten salt in a 1:1 ratio. And then whole the acquired pigments were calcined at 700 ℃ for 30 min in air to remove the uncovered CB to gain the C@$ZrSiO_4$ black pigment.

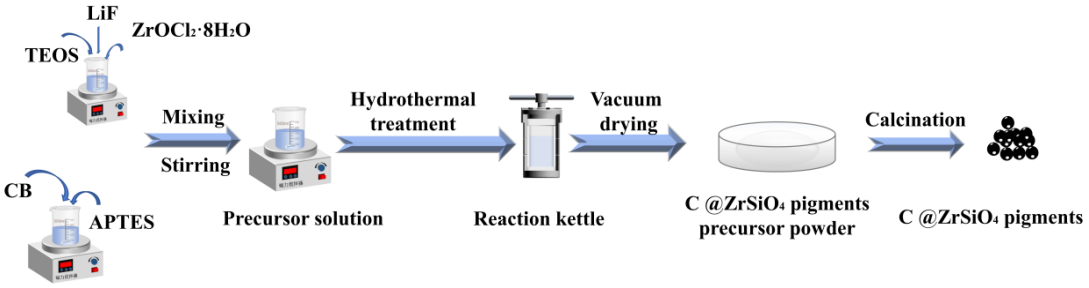

Figure 1. Process flow chart of synthesis C@$ZrSiO_4$ pigment

Characterization

The composition of the sample was analyzed by bruker D8 Advance diffractometer. The morphology of the samples were found by operating a JSM-6700F scanning electron microscope (SEM) with energy dispersive X-ray spectroscopy (EDS) field emission and a JEM-2010 transmission electron microscope (TEM). The bond formation of the samples were tested by XPS (XPS, Thermo Scientific ESCALAB 250Xi). Raman spectroscopy is obtained with a Raman spectrometer (at Via, Renishaw, UK). Ultraviolet-visible diffuse reflectance spectroscopy (UV-Vis-DRS) was obtained on the Nicolet 5700 infrared spectrometer. The CIE-*L*a*b** parameters of the sample are recorded by the automatic WSD-3C color system.

RESULTS AND DISCUSSION

Characterization of Mesoporous $ZrSiO_4$

Initial studies were carried out on the mesoporous $ZrSiO_4$ synthesized by hydrothermal method. So as to obtain the $ZrSiO_4$ morphology information, SEM and TEM were used to analyze the samples. SEM images were taken which clearly shows that it is composed of grain with consistent morphology (corresponding to that there is only one pure crystal phase of $ZrSiO_4$ in XRD), and the size of the prepared powder is similar (with a diameter of about 1 μm), as shown in Figure 2a, which is regular morphology and high dispersion. Figure 2b shows the TEM photograph of sample, which further prove the layered structure of $ZrSiO_4$ (consistent with SEM results). Figure 2c shows the marginal region of sample, and it can be seen that the surface is composed of many small grains. Figure 2d shows the XRD pattern of sample, which can be seen from the figure that the powder prepared under hydrothermal conditions can generate pure phase $ZrSiO_4$, and each crystal matches the standard spectrum (JCPDS NO. 06-0266). Figure 2e further magnifies Figure 2c and selects the specified area for structure analysis. The crystal lattice fringes can be observed clearly in the figure, indicating that the sample has a relatively complete crystallinity. The measured crystal face spacing is 0.326 nm and 0.439 nm, respectively, vesting in the (411) and (512) crystal faces of $ZrSiO_4$ crystal. Figure 2f shows the polycrystalline diffraction pattern of $ZrSiO_4$, corresponding to (200), (220), (301) and (411) crystal planes of $ZrSiO_4$ crystal, respectively.

To further analyze the surface structure of $ZrSiO_4$. Figure 2g shows the isothermal curve of N_2 adsorption and desorption of $ZrSiO_4$. Tubular channels exist on surface of $ZrSiO_4$. The isotherm shows an adsorption hysteresis loop of relative partial pressure (P/P_0) from 0.4 to 1.0, which corresponds to the capillary condensation system occurring in porous adsorbent[5, 6]. On the basis of the IUPAC classification, the hysteresis loop be part of type IV, and the figure also shows that the average aperture is about 5nm, which is a mesoporous structure. In conclusion, it can be determined that the $ZrSiO_4$ prepared by hydrothermal method is mesoporous $ZrSiO_4$ with special structure, and its high specific surface area reaches 322.4805 m^2/g, which gives it strong adsorption capacity. The CB can be adsorbed in mesoporous $ZrSiO_4$. The $ZrSiO_4$ are secondary grown by heat treatment, thus

the CB is tightly wrapped by $ZrSiO_4$ grains. In summary, it can be concluded that the $ZrSiO_4$ prepared by hydrothermal method is a layered porous particle composed of polycrystals with a particle diameter of about 1 μm, which is conducive for subsequent encapsulation.

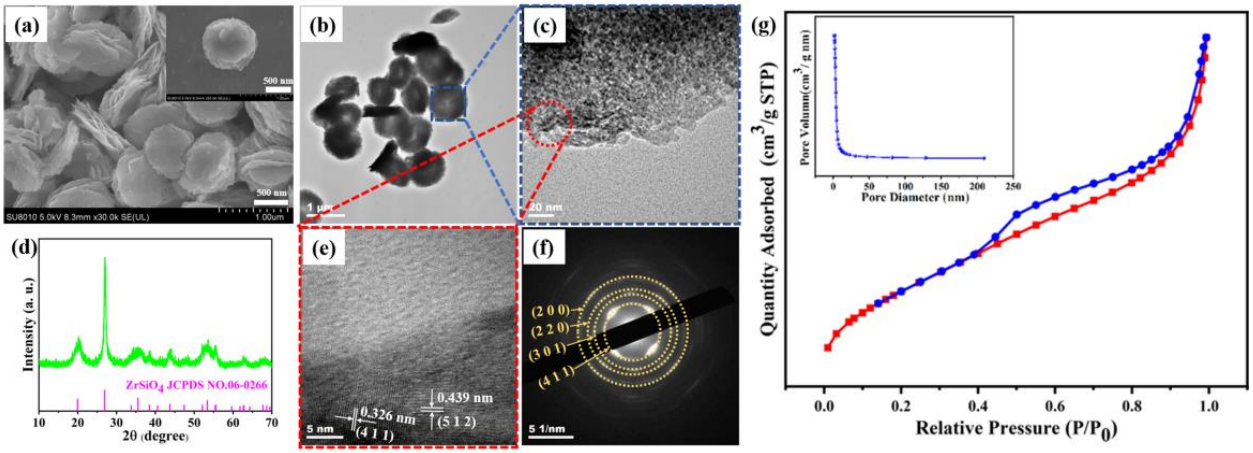

Figure 2. (a) SEM image; (b, c) TEM images; (d) XRD pattern; (e) HR-TEM image; (f) SAED pattern; (g) isothermal curve of N_2 adsorption and desorption of the Zirconium silicate precursor

Characterization of C@$ZrSiO_4$

The XRD patterns of different APTES dosages with or without molten salt assistance at 900 ℃ in Figure 3(a, b). The peak intensity of the samples were relatively high, which match the $ZrSiO_4$ (JCPDS 06-0266) phase. When APTES/Zr is 0.7152, SiO_2 crystal phase appears, which is because APTES itself contains Si atoms. Although excess Si will be discharged with SiF_4 gas, when APTES dosage is too high, the solubility of Si atoms is high, resulting in some Si atoms not being able to escape with SiF_4 gas.

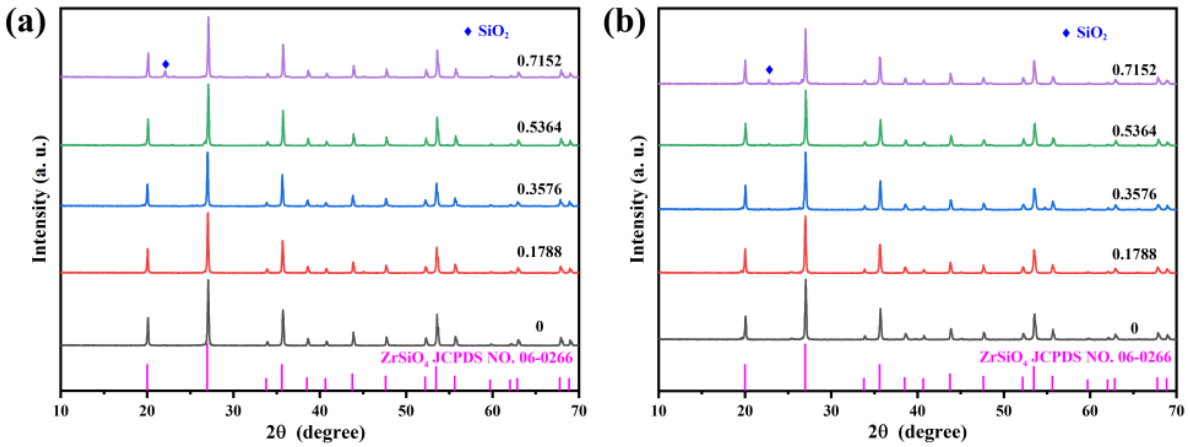

Figure 3. XRD pattern of samples with APTES at different content (a) without; and (b) with molten saltassistance

Figure 4(a, b) showed SEM images of CB and mesoporous $ZrSiO_4$ prepared by hydrothermal method, it could be spoted that the as-synthesized mesoporous $ZrSiO_4$ sample acted out highly monodispersive stratiform porous particle with a neatly arranged surface and the diameter of particle is about 1 μm. Compared to Wang et al[7]. the collapse of mesoporous ZrO_2 eliminates the process of reacting with SiO_2 and prevents SiO_2 encapsulation. At the same time, to explore this impact of mesoporous $ZrSiO_4$ on synthesis of C@$ZrSiO_4$ pigment. The typical SEM micrographs of the hydrothermal synthesis into the C/$ZrSiO_4$ precursor and C@$ZrSiO_4$ pigment formed after the C/$ZrSiO_4$ precursor was calcined at 900 ℃ with molten salt was displayed in Figure 4(c, d), respectively, It can be seen that CB is adsorbed in mesoporous $ZrSiO_4$ with high specific surface area (Figure 4c), which is successfully encapsulated in the $ZrSiO_4$ crystal particles after heat treatment (Figure 4d). In summary, under the condition of calcination at 900 ℃, the CB is successfully encapsulated through the accumulation of grains.

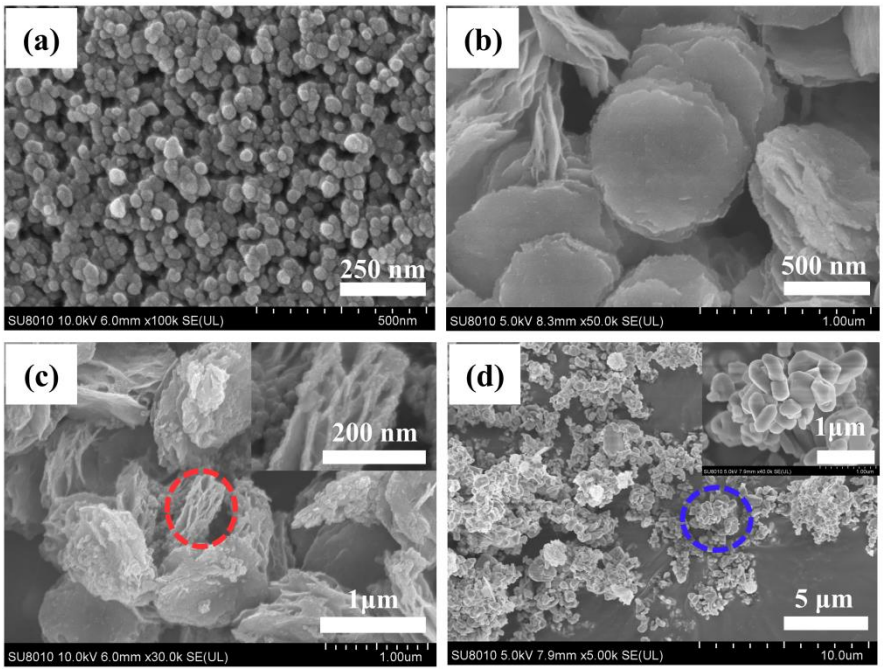

Figure 4. SEM images of(a) CB suspension; (b) $ZrSiO_4$ precursor powder; (c) C/$ZrSiO_4$ precursor powder; (d) C@$ZrSiO_4$ pigment

Figure 5 illustrates the TEM photos, EDS energy spectrum, the selected electron diffraction and EDS surface scanning of C@$ZrSiO_4$ pigment, respectively. The TEM images (Figure 5(a, b)) reveal that CB is wrapped in the gaps of $ZrSiO_4$ grains, Compared to Chen et al[8]. molten salts play a denser role here. The EDS demonstrates the uniform distribution of Zr, Si, O and C elements (Figure 5c). So as to further accurately determine that the particles are $ZrSiO_4$ crystals. As shown in Figure 5d, the interplanar clearance was estimated to be around 0.322 nm. In addition, the SAED pattern also agrees with the HRTEM result, showing the diffractive crystal plane assignable to (301), (512), and (220) planes of $ZrSiO_4$ crystal (Figure 5e). Besides, the relative content of carbon tested in EDS spectrum is 33.44%. in Figure 5f.

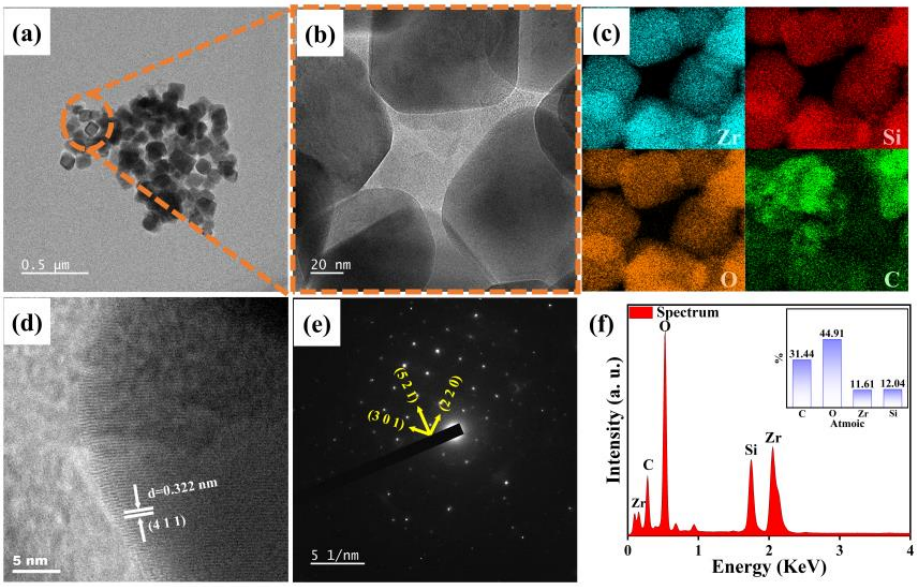

Figure 5. (a, b) TEM images ;(c) EDS mapping of, Zr, Si, O, C ; (d) HR-TEM image ; (e) SAED pattern; (f)and EDS spectrum of C@$ZrSiO_4$ pigment

As perceived in Figure 6a, the chromaticity value of the pigment is significantly reduced. the chromaticity value is the lowest when APTES/Zr is 0.7152(L^*=68.59). By forming new bonds between APTES and CB, it is more advantageous for CB to be encapsulated by $ZrSiO_4$[9]. After adding molten salt in Figure 6b, the content of APTES gradually increased, the L^* value

displayed of first declining and then rising, which was consistent with the result without the addition of molten salt, and when APTES/Zr is 0.5364, the chroma value reached the lowest (L^*=27.65). Compared to Chen et al. use of APTES, the chromaticity value has been further improved. The addition of molten salt promotes the densification of $ZrSiO_4$ inclusion[10]. Within the visible wavelength range of 380 ~ 750 nm, when APTES/Zr is 0.5364, the light absorption performance of the prepared powder is the best, indicating that the light ray enters the crystal interface, and is absorbed by reflection and refraction, which is accord with the result of L^* value, as shown in Figure 6c.

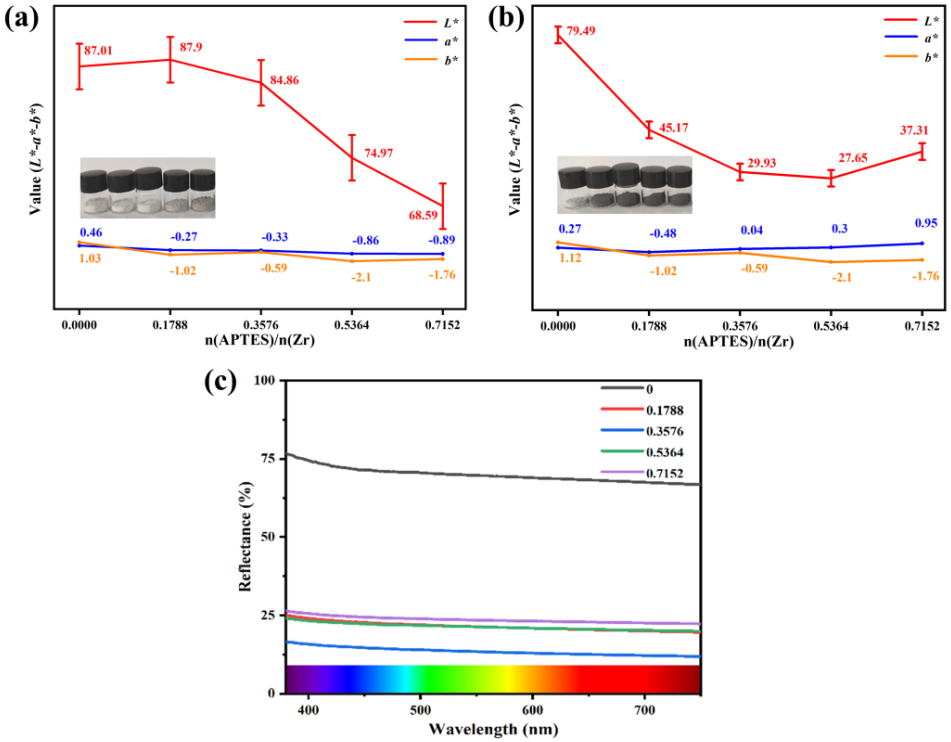

Figure 6. The Chromaticity curve of different APTES dosage (a) without (b) and with molten salt assistance: L^* a^* b^* value; (c) UV-visible diffuse reflection absorption spectra of C@$ZrSiO_4$ pigment

To study the properties of pigment that it is evaluated by applying pigment to transparent glazes. Figure 7 shows digital photos of different pigment additive amounts applied to the basic glaze (900 °C). Table 1 show the chromaticity values. As the pigment additive amount increases, the glaze gradually turns black, and the glaze is smooth and flat, with a good decorative effect on the glaze.

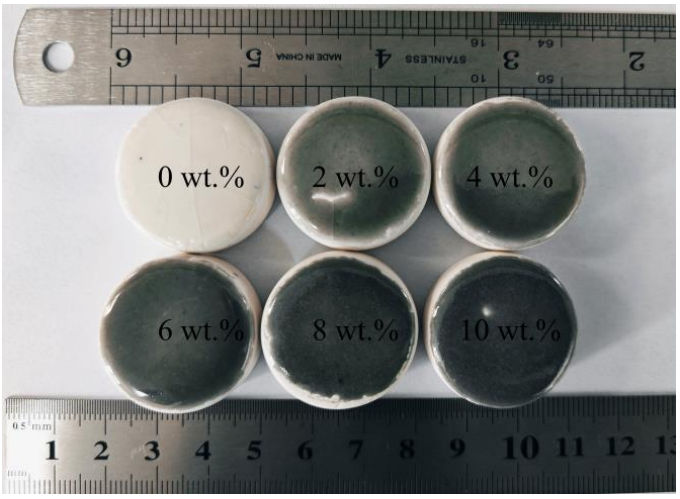

Figure 7. Digital photos of different pigments addition amount applied to the base glaze sample

Table 1. *L*-a*-b** values of different pigments additive amounts in glaze

Additive amounts (wt. %)	CIE		
	*L**	*a**	*b**
2	54.84	-0.60	2.11
4	50.88	-0.69	1.10
6	46.01	0.12	7.46
8	44.11	0.00	1.21
10	43.23	0.27	0.45

To further confirm that CB is successfully encapsulated by $ZrSiO_4$, Raman spectroscopy can characterize the structural information of materials. Figure 8 reveals the Raman spectra of mesoporous $ZrSiO_4$ powder and pigment with and without the molten salt. In 1006 and 967 cm^{-1} cm^{-1} appeared two peaks, respectively corresponding to Zr-O-Si asymmetric and symmetric stretching modes[11]. The peak at position 434 cm^{-1} corresponds to O-Si-O. Meantime, the characteristic peak D band (1358 cm^{-1}) and G band (1590 cm^{-1}) occured in C@$ZrSiO_4$ pigment[12]. The semi-quantitative analysis by Raman spectroscopy according to the Gaussian distribution, the $ZrSiO_4$ pigment is divided into two characteristic peaks, the peak area represent the content of the substance and the peak areas are 84196 and 530775 respectively. After the introduction of molten salt, the carbon content is much higher than that of the pigment without molten salt, which proves that molten salt is conducive to the encapsulation of CB.

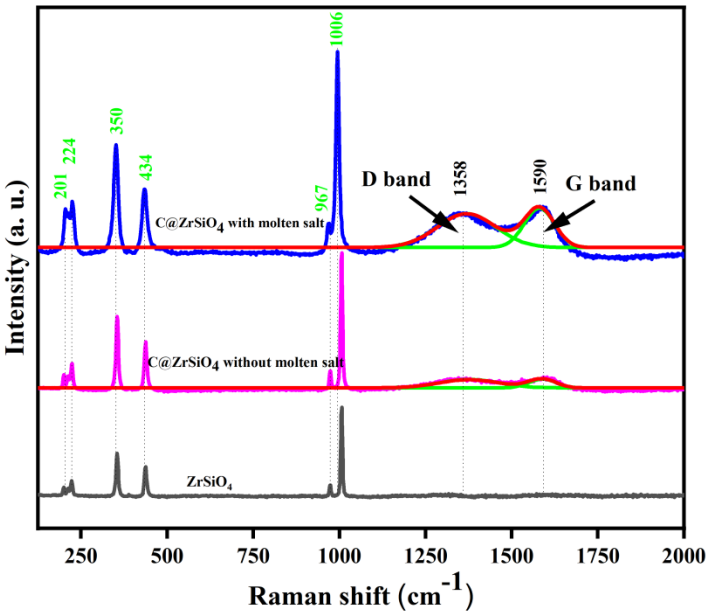

Figure 8. Raman spectra of $ZrSiO_4$ powder, C@$ZrSiO_4$ pigment with and without molten salt

In order to further study the relationship between sample elements, component analysis was conducted by XPS. As indicated in Figure. 9a, C1s, O1s, Zr3d and Si2p peaks were detected in the XPS survey, the characteristic peaks of other elements are not obvious. From the spectra, the elements detected on the surface of the substance and a semi-quantitative analysis of them was shown in Figure. 9a. The typical XPS fine spectra of $ZrSiO_4$ is shown in Figure. 9 (b ~ e). Figure. 9b shows a subset of the spectrum focused on the C1s peak, vesting in C-C and Zr-O-C at ~284.78 eV and ~286.28 eV positions, respectively[13]. Further analysis of C1s spectra shows $ZrSiO_4$ and CB can be bonded thought chemical bond. Meanwhile, Figure. 9(c, d) show a subset of two spectra focused on O1s and Zr3d peaks respectively, which were related to Zr-O together, assisted in verifying the Zr-O-C bond. In the Si 2p spectrum (Figure. 9(e)), the peak mainly centered at ~102.98 eV corresponded to Si-O-C[14]. Combined with the above analysis, it is not difficult to see that the CB surface is covered by $ZrSiO_4$ after calcination at 900 °C (which additionally confirmed the results of SEM and TEM). $ZrSiO_4$ forms a closed inclusion structure around the CB and ensures that the CB can still have excellent tinting performance after high temperature. Table 2 shows the XPS fitting results of the synthesized inclusion pigment.

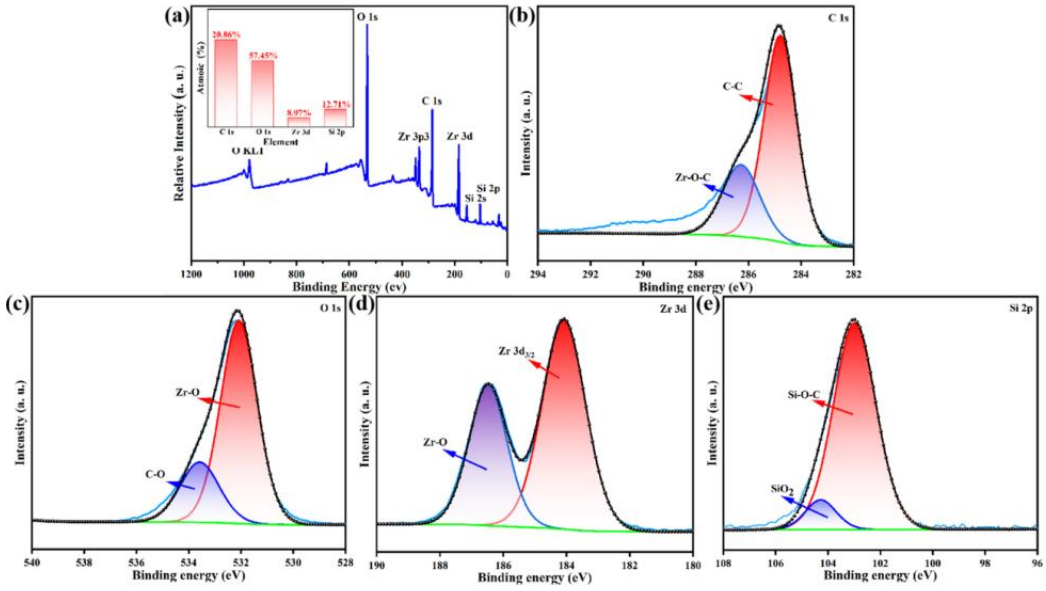

Figure 9. The XPS spectra of C@$ZrSiO_4$ black pigment: (a) survey; (b) C 1s; (c) O 1s; (d) Zr 3d; (e) Si 2p

Table 2. The XPS fitting results of the synthesized inclusion pigment

parameter	C 1s			O 1s			Zr 3d			Si 2p	
	C-C	Zr-O-C		Zr-O	C-O		$Zr\ 3d_{3/2}$	Zr-O		Si-O-C	SiO_2
BE (eV)	284.78	286.28		532.08	533.58		184.08	186.48		102.98	104.28
area	118289.79	47107.20		230686.23	73126.68		108039.15	63813.92		30636.05	3179.37

The synthesis mechanism diagram of C@$ZrSiO_4$ black pigment is displayed in Figure 10. When CB is treated with APTES can improve the adhesion between CB and $ZrSiO_4$[4], which is more conducive to the encapsulation of CB. Polycrystalline mesoporous layered $ZrSiO_4$ is heat treated to form a single $ZrSiO_4$, and the gaps between the particles provide a good inclusion site for CB. The synergistic effect of the synergistic effect of mechanisms encouraged the synthesis of C@$ZrSiO_4$ black pigment.

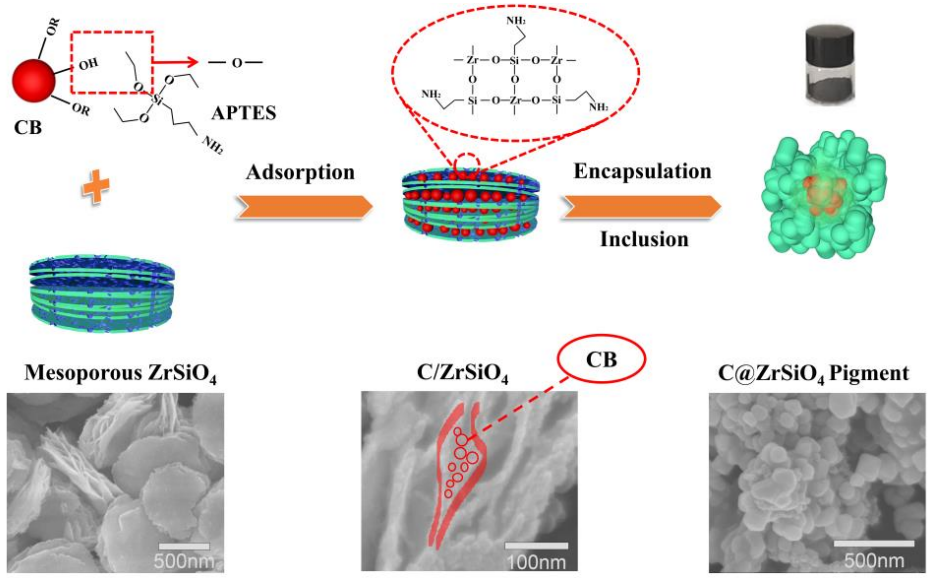

Figure 10. Schematic diagram for C@$ZrSiO_4$ preparation via layered porous framework

CONCLUSIONS

In this paper, C@$ZrSiO_4$ black pigment was successfully synthesized by mesoporous collapse method. The APTES promotes the connection between $ZrSiO_4$ and CB, which improved the encapsulation efficiency of CB, which the chroma value reduced

to 27.65. And it can show better performance at high temperatures. However, its color performance still has some room for improvement. Therefore, it is particularly important to further explore the performance in the future.

ACKNOWLEDGEMENT

This work was supported by the National Natural Science Foundation of China [grant numbers 52362041, 52262003]; Jiangxi Provincial Natural Science Foundation [grant numbers 20242BAB20166, 20232ACB204012, 20232BAB204031]; the Training Program for Academic and Technical Leaders of Major Disciplines in Jiangxi Province [grant numbers 20243BCE51117]; the Jingdezhen Science and Technology plan project [grant numbers 20202GYZD013-14, 20212GYZD009-06, 20224GY008-07, 20224GY008-13]

REFERENCES

[1] M. Monia, M. Consuelo, P. Alessio, A. Andrea, M. Fabrizio, F. Ludovica, C. Raffaele, M. Tiziano, Improvement of color quality and reduction of defects in the ink jet-printing technology for ceramic tiles production: A Design of Experiments study. Ceramics International, 2016, 42(1): 1459-1469.

[2] S. L. Chen, M. T. Cheng, Y. Lang, H. K. Wei, C. A. Wang, Synthesis and chromatic properties of zircon encapsulated ceramic black pigment with carbon sphere as carbon source, Journal of the European Ceramic Society, 2018, 38(4): 2218-2227.

[3] C. Peng, C. X. Zhang, M. Lv, Preparation of silica encapsulated carbon black with high thermal stability, Ceramics International, 2013, 39(6): 7247-7253.

[4] T. Chen, X. J. Zhang, W. H. Jiang, J. M. Liu, W. Jiang, Z. X. Xie, Synthesis and application of C@$ZrSiO_4$ inclusion ceramic pigment from cotton cellulose as a colorant, Journal of the European Ceramic Society, 2016, 36(7): 1811-1820.

[5] Q. K. Wang, Q. B. Chang, K. Yang, Y. Q. Wang, X. Li, J. E.Zhou, Relationship of Preparation Parameters and Chromatic Properties of Zircon-Encapsulated Carbon Black Ceramic Pigment Prepared with a Sol-Gel-Spraying Method, Journal of Ceramic Science and Technology, 2017, 8(2): 287-294.

[6] Y. Ding, Q. Xian, Z. D. Jiang, L. Chen, T. H. Xiong, X. M. He, W. P. Yang, H. Dan, Tao. Duan, Immobilization of uranium in cristobalite ceramic through adsorption on mesoporous SBA-15 and further sintering process, Journal of the European Ceramic Society, 2020, 40(5): 2113-2119.

[7] Q. K. Wang, Q. B. Chang, Y. Q. Wang, X. Wang, J. E. Zhou, Preparation of Zircon-Encapsulated Carbon Black Ceramic Pigment Using the Collapsed Mesoporous-Structure, Silicon, 2018, 10(5): 2253-2262.

[8] T. Chen a, X. J. Zhang, W. H. Jiang, Z. X. Xie, Y. Q. Xu, H. D. Tang, W. Jiang, Molten-salt assisted synthesis and characterization of $ZrSiO_4$ coated carbon core-shell structure pigment, Advanced Powder Technology, 2020, 31(6): 2197-2206.

[9] X. X. Kong, J. H. Liu, S. M. Li, M. Yu, APTES-modified graphene oxide loaded with cerium dibutylphosphate as two-Dimensional nanocomposites for enhancing corrosion protection properties, Corrosion Science, 2023: 213(0): 110966.

[10] A. A. Ballman, R. A. Laudise, Crystallization and solubility of zircon and phenacite in certain molten salts, Journal of the American Ceramic Society, 1965, 48(3): 130-133.

[11] C. Zhang, J. You, H. Chen, H. Zeng, G. Jiang, Vibrational modes and in-situ high temperature Raman spectra of zircon, Journal of the Chinese Ceramic Society. 2006, 34(10): 1172-1176.

[12] X. Y. Zhu, H. F. Qiu, P. Chen, G. Z. Chen, W. X. Min, Graphitic carbon nitride (g-C_3N_4) in situ polymerization to synthesize MOF-Co@CNTs as efficient electromagnetic microwave absorption materials[J]. Carbon, 2021, 176(0): 530-539.

[13] S. R. Teeparthi, E. W. Awin, R. Kumar, Dominating role of crystal structure over defect chemistry in black and white zirconia on visible light photocatalytic activity, Scientific reports, 2018, 8(1): 1-11.

[14] R. Colomaribera, R. W. E. Vandekruijs, J. M. Sturm, A. E. Yakshin, F. Bijkerk, Intermixing and thermal oxidation of ZrO_2 thin films grown on a-Si, SiN, and SiO_2 by metallic and oxidic mode magnetron sputtering, Journal of Applied Physics, 2017, 121(11): 115303-1-115303-13.